# Increased computational accuracy in multi-compartmental cable models by a novel approach for precise point process localization

**A.E. Lindsay**
Department of Mathematics, University of Edinburgh,
Edinburgh EH9 3JZ

**K.A. Lindsay**
Department of Mathematics, University of Glasgow,
Glasgow G12 8QQ

**J.R. Rosenberg**[†]
Division of Neuroscience and Biomedical Systems,
University of Glasgow, Glasgow G12 8QQ

October 26, 2004

[†] **Corresponding author**

J.R. Rosenberg
West Medical Building
Division of Neuroscience and Biomedical Systems
University of Glasgow
Glasgow G12 8QQ
Scotland UK

Tel (+44) 141 330 6589
Fax (+44) 141 330 2923
Email `j.rosenberg@bio.gla.ac.uk`

**Keywords**

Compartmental models, Dendrites, Cable Equation

**Abstract**

Compartmental models of dendrites are the most widely used tool for investigating their electrical behaviour. Traditional models assign a single potential to a compartment. This potential is associated with the membrane potential at the centre of the segment represented by the compartment. All input to that segment, independent of its location on the segment, is assumed to act at the centre of the segment with the potential of the compartment. By contrast, the compartmental model introduced in this article assigns a potential to each end of a segment, and takes into account the location of input to a segment on the model solution by partitioning the effect of this input between the axial currents at the proximal and distal boundaries of segments. For a given neuron, the new and traditional approaches to compartmental modelling use the same number of locations at which the membrane potential is to be determined, and lead to ordinary differential equations that are structurally identical. However, the solution achieved by the new approach gives an order of magnitude better accuracy and precision than that achieved by the latter in the presence of point process input.

# 1 Introduction

Compartmental models have become important tools for investigating the behaviour of neurons to the extent that a number of packages exist to facilitate their implementation (*e.g.* Hines and Carnevale 1997; Bower and Beeman 1997). These models are constructed by replacing the continuum description of a neuron by a discrete description of the neuron formed by partitioning it into contiguous segments which interact with their nearest neighbours across common boundaries. A compartment is a mathematical representation of the morphological and biophysical properties of a segment, and a compartmental model is the collection of all compartments along with a specification of their connectivity. The efficacy of any formulation of a compartmental model depends on the faithfulness with which it captures the behaviour of the neuron that it represents, and it is in this respect that the new compartmental model developed in this article will be seen to perform better than existing compartmental models with a similar level of complexity.

The traditional approach to compartmental modelling (*e.g.*, Rall 1964; Segev and Burke, 1998) assigns a single potential to a compartment. This potential takes its value through an association with the average value of the current density crossing the membrane of the segment, and in a traditional compartmental model is approximated by the membrane potential at the centre of the segment. However a compartment of this type is aesthetically unsatisfactory since it cannot act as the fundamental unit in the construction of a model dendrite, first, because two compartments are required to define axial current flow, and second, because half compartments are required to represent branch points and dendritic terminals. On the other hand, the new approach to compartmental modelling assigns two potentials to a compartment – one to represent the membrane potential at the proximal boundary of the segment and the other to represent the membrane potential at its distal boundary. The new compartment can exist as an independent entity and can therefore function as the basic building block of a multi-compartmental neuronal model. Another significant difference between a traditional compartmental model and the new compartmental model lies in the novel procedure for the treatment of transmembrane current. In a traditional compartmental model the influence of transmembrane current on a segment is approximated by requiring these currents to act at the centre of the segment with the single potential assigned to the compartment representing the segment, and consequently these models do not reflect accurately the influence of the precise location of point process input[1] on the segment. By contrast, the formulation of the new compartmental model makes it more responsive to the influence of the location of point process input to a segment, and in the presence of these inputs, is shown to be an order of magnitude more accurate that a comparable traditional compartmental model.

The accuracy of the new and traditional approaches to compartmental modelling is first assessed

[1]Following the terminology of Hines and Carnevale (1997), a point process is taken to mean either synaptic input (voltage-dependent) or an exogenous point current input (voltage-independent).

by calculating the error in the somal potential of a test neuron when each approach is used to calculate this potential ten milliseconds after the initiation of large scale point current input. In a second comparison, the accuracy of the two approaches is assessed by comparing the statistics of the spike train output generated by each type of compartmental model of the test neuron when subjected to large scale synaptic input.

## 2 Structure of compartmental models

We are concerned with compartmental models of dendrites. In this context, the fundamental morphological unit is the dendritic *section*, defined to be the length of dendrite connecting one branch point to a neighbouring branch point, to the soma or to a terminal. Compartmental modelling begins by subdividing each dendritic section into segments which are typically regarded as uniform circular cylinders (*e.g.* Segev and Burke, 1998) or tapered circular cylinders (Hines and Carnevale, 1997). In the new approach to compartmental modelling, the known membrane potentials at the ends of a segment (rather than its centre) provide the basis for the development of a set of rules which enable the influence of precisely located point process input to be partitioned between the axial current at the proximal and distal boundaries of the segment. The mathematical equations of the compartmental model are constructed by enforcing conservation of axial current at segment boundaries, dendritic branch points and dendritic terminals.

### 2.1 Model accuracy and the partitioning of point process input

The benefit in accuracy gained by taking into account the precise placement of point process input on a dendrite is best appreciated by considering how, in the absence of this facility, small variations in the location of segment boundaries exert a large influence on the solution of a traditional compartmental model. Consider, for example, a point process close to a segment boundary. A small change in the position of that boundary may move the assigned location of this point process from the centre of one segment to that of an adjacent segment. With respect to a traditional compartmental model, the location of this point process is therefore determined only to an accuracy of half a segment length, and this indeterminacy will in turn generate a model solution that is particularly sensitive to segment boundaries. Of course, with a small number of point process input, this problem can be avoided in the traditional approach to compartmental modelling by arranging that only one point process falls on a segment, and that the location of this input coincides with the centre of the segment. However, this strategy is not feasible when dealing with large scale point process input. What is required is a procedure which describes the effect of point process input on a dendritic section in a way that is largely insensitive to how that section is represented by segments.

The primary sources of error in the construction of a compartmental model are the well-

documented effect of discretising a continuous dendrite, and the less well-documented error introduced by the placement of point process input on the dendrite. In the traditional approach based on a compartmental model with $n$ compartments, the first type of error is $O(1/n^2)$ (by analogy with the finite difference representation of derivatives), but it is not widely recognised that the second type of error is $O(1/n)$ whenever the input does not naturally fall at the centre of segments. Since the accuracy of any model is governed by the least accurate contribution to the model, it is clear that *in practice* the traditional approach to compartmental modelling in the presence of point current and synaptic input is $O(1/n)$ accurate. This theoretical observation is supported by the simulation studies of Subsections 5.2 and 5.3, and by an example provided for us by an anonymous reviewer. This reviewer used the simulator NEURON to calculate the somal potential of the test neuron shown in Figure 3 10msec after the initiation of point current input. The results of this calculation are shown in Table 1

| Segments per branch *section* | Point current input at centre of nearest segment | | Point current input divided proportionately | |
|---|---|---|---|---|
| | $V$ (mV) | $\Delta V$ (mV) | $V$ (mV) | $\Delta V$ (mV) |
| 1 | 10.2355 | | 10.5692 | |
| 2 | 10.2311 | $(-4.4616 \times 10^{-3})$ | 10.3357 | $(-2.3352 \times 10^{-1})$ |
| 4 | 10.2367 | $(5.6256 \times 10^{-3})$ | 10.2725 | $(-6.3143 \times 10^{-2})$ |
| 8 | 10.2333 | $(-3.4428 \times 10^{-3})$ | 10.2556 | $(-1.6908 \times 10^{-2})$ |
| 16 | 10.2470 | $(1.3754 \times 10^{-2})$ | 10.2519 | $(-3.6550 \times 10^{-3})$ |
| 32 | 10.2509 | $(3.8793 \times 10^{-3})$ | 10.2508 | $(-1.1320 \times 10^{-3})$ |
| 64 | 10.2521 | $(1.1874 \times 10^{-3})$ | 10.2506 | $(-2.4666 \times 10^{-4})$ |
| 128 | 10.2530 | $(8.8765 \times 10^{-4})$ | 10.2505 | $(-6.3146 \times 10^{-5})$ |
| 256 | 10.2511 | $(-1.9053 \times 10^{-3})$ | 10.2505 | $(-1.5181 \times 10^{-5})$ |

Table 1: The somal potential of the test neuron shown in Figure 3 is given 10msec after the initiation of point current input. The calculation is done for nine different levels of discretisation and two methods for the placement of exogenous point current input.

The results shown in the middle panel of Table 1 (traditional compartmental model) are based on placing the exogenous point current input at the centre of its nearest segment, whereas the results shown in the right hand panel (modified compartmental model) are based on the division of the point current input between the centres of adjacent compartments in proportion to the conductance between the location of the input and these centres. Several important differences between the two procedures for allocating the location of point current input are evident from the results set out in Table 1. The results based on dividing the current proportionately between the centres of neighbouring compartments converge smoothly and more rapidly to the true potential than those based on the traditional approach in which the current is placed at the centre of the compartment. An extrapolation procedure demonstrates that the potentials

generated by the modified approach converge quadratically to the true somal potential as the number of compartments is increased. Moreover, not only does the solution following the traditional approach (middle panel) converge to the true potential more slowly than the modified approach (right hand panel), the former appears to oscillate as it approaches this potential. Finally, further evidence for the superior convergence of the modified approach is clear from the observation that the best estimate of the true potential using the traditional approach with 256 segments per branch section is achieved in the modified approach with approximately 28 segments per branch section. It will be seen in Section 4.1 that the procedure used by the reviewer to partition point current input is a special case of the general procedure for partitioning point process input. By contrast with the traditional approach, the new approach to compartmental modelling describes the influence of point process input to an accuracy of $O(1/n^2)$, and therefore one would anticipate that it does not degrade the overall accuracy of the model. The validity of this assertion is demonstrated through the simulation studies in Subsections 5.2 and 5.3.

# 3 Distributed and point process input to a segment

In general, segments receive distributed and point process sources of input each of which require a different mathematical treatment. The current supplied by distributed input such as intrinsic voltage-dependent current or capacitative current is proportional to the surface area of the segment on which it acts, whereas the current supplied to a segment at a synapse or by an exogenous point input is independent of the size of the segment. An implicit assumption of a compartmental model is that distributed current input to a segment is small by comparison with axial current flowing along the segment.

To appreciate why this assumption is reasonable, consider a cylindrical dendritic segment of radius $r$ (cm), length $h$ (cm) and with membrane of constant conductance $g_{\mathrm{M}}$ (mS/cm$^2$). Suppose that axoplasm has constant conductance $g_{\mathrm{A}}$ (mS/cm) and that a potential difference $V$ (mV) exists between the segment boundaries, then the axial current along the segment is $I_{\mathrm{A}} = \pi r^2 g_{\mathrm{A}} V/h$ ($\mu$A) and the total distributed current crossing the membrane of the segment is $I_{\mathrm{M}} = 2\pi r h g_{\mathrm{M}}\,(V/2)$. The ratio of the distributed current to the axial current is therefore

$$\frac{\text{Distributed current}}{\text{Axial current}} = \frac{I_{\mathrm{M}}}{I_{\mathrm{A}}} = \frac{\pi r h g_{\mathrm{M}}\, V}{\pi r^2 g_{\mathrm{A}}\,(V/h)} = \frac{h^2 g_{\mathrm{M}}}{r g_{\mathrm{A}}} = \left(\frac{h}{r}\right)^2 \frac{r g_{\mathrm{M}}}{g_{\mathrm{A}}}\,. \tag{1}$$

For a typical dendritic segment $r g_{\mathrm{M}}/g_{\mathrm{A}}$ is small (say $\approx 10^{-5}$), and therefore distributed current acting on a segment is small by comparison with axial current for "short" segments. On the other hand, segments several orders of magnitude longer than their radius can be expected to have distributed and axial currents of similar magnitude. An important property of a compartmental model is that segments are not excessively long by comparison with their radius. (However, see Segev and Burke, 1998, Figure 3.3b). In the treatment of distributed current, the development of the new compartmental model makes explicit use of the assumption that distributed current is much smaller than axial current. This assumption may not be valid for point process input, and

will not be made for the treatment of this type of input in the new approach to compartmental modelling.

### 3.1 Axial current in the absence of transmembrane current

The importance of the conclusion from Section 3 is that distributed transmembrane current acting on short segments is small compared with axial current, and may be neglected in a first approximation of the distribution of membrane potential on a segment. Thus in the absence of point process input, the axial current in a segment is well approximated from the potential drop across the segment. In the light of this approximation, consider Figure 1 which illustrates a dendritic segment of length $h$ in which $\lambda \in [0,1]$ is the fractional distance of a point of the segment from its proximal end ($\lambda = 0$). Let $r_{\rm P}$ and $r_{\rm D}$ be the radii of the segment at its proximal and distal boundaries respectively, let $V_{\rm P}(t)$ and $V_{\rm D}(t)$ be the membrane potentials at these boundaries and let $I_{\rm PD}$ be the axial current in the segment in the absence of transmembrane current.

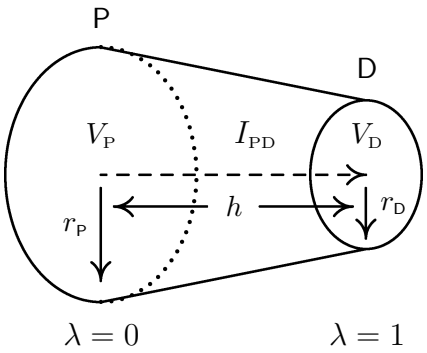


Figure 1: A segment of length $h$ is illustrated. In the absence of transmembrane current, membrane potentials $V_{\rm P}$ and $V_{\rm D}$ at the proximal and distal boundaries of the segment generate axial current $I_{\rm PD}$.

The membrane of the segment in Figure 1 is formed by rotating the straight line PD about the axis of the dendrite to form the frustum of a cone of radius

$$r(\lambda) = (1-\lambda)r_{\rm P} + \lambda r_{\rm D}\,, \qquad \lambda \in [0,1]\,. \tag{2}$$

Assuming that the segment is filled with axoplasm of constant conductance $g_{\rm A}$ and that no current crosses its membrane, then the relationship between $V_{\rm P}$, $V_{\rm D}$ and $I_{\rm PD}$ can be constructed by integrating the defining equation of axial current, namely $I_{\rm PD} = -g_{\rm A}\, A(x)\, dV/dx$, from the proximal to the distal boundary of a segment. For the conical segment illustrated in Figure 1, $A(x) = \pi r^2(\lambda)$, $dV/dx = h^{-1}\, dV/d\lambda$ and the equation to be integrated is

$$I_{\rm PD} = -\frac{g_{\rm A}\pi}{h}\Big[\,(1-\lambda)r_{\rm P} + \lambda r_{\rm D}\,\Big]^2\,\frac{dV}{d\lambda}$$

with boundary conditions $V(0) = V_{\rm P}$ and $V(1) = V_{\rm D}$. The result of this calculation is that the the axial current $I_{\rm PD}$ and the potentials $V_{\rm P}$ and $V_{\rm D}$ are connected by the formula

$$I_{\rm PD} = \frac{\pi g_{\rm A} r_{\rm P} r_{\rm D}}{h}\,(\,V_{\rm P} - V_{\rm D}\,) \tag{3}$$

in the absence of transmembrane current. Moreover, the potential at the point $\lambda$ is

$$V(\lambda) = \frac{V_{\rm P}\,(1-\lambda)\,r_{\rm P} + V_{\rm D}\,\lambda\,r_{\rm D}}{(1-\lambda)\,r_{\rm P} + \lambda\,r_{\rm D}}\,. \tag{4}$$

Note that equation (4) is valid for sections with taper and in the absence of taper will lead to a membrane potential which varies linearly along the length of a segment. The subsequent development of the new compartmental model assumes that sections may taper unless stated specifically that the section is uniform.

### 3.2 Partitioning rule for transmembrane current

In compartmental modelling the effect of transmembrane current is represented in the model by input at points, or nodes, at which the membrane potential is known. In a traditional approach to compartmental modelling, these nodes are at the centre of segments, whereas in the new approach they are located at the boundaries of segments. The new approach partitions the effect of input at any location between the nodes at the proximal and distal boundaries of the segment. This procedure ensures that the solution of the compartmental model is insensitive to small changes in the location of segment boundaries because changes in these boundaries also affect how the input is partitioned between nodes. In the mathematical description of the new compartmental model, the effect of input to a segment is treated as perturbations $I_{\rm P}$ and $I_{\rm D}$ to the axial current $I_{\rm PD}$ at the proximal and distal boundaries of a segment. Axial current $I_{\rm PD} + I_{\rm P}$ is assumed to leave the proximal boundary of a segment in the direction of its distal boundary, while axial current $I_{\rm PD} + I_{\rm D}$ is assumed to arrive at the distal boundary of a segment from the direction of its proximal boundary. The perturbations $I_{\rm P}$ and $I_{\rm D}$ must satisfy the conservation of current condition

$$(I_{\rm PD} + I_{\rm D}) - (I_{\rm PD} + I_{\rm P}) + h\int_0^1 J(\lambda,t)\,d\lambda = 0 \quad \rightarrow \quad I_{\rm P} - I_{\rm D} = h\int_0^1 J(\lambda,t)\,d\lambda \tag{5}$$

where $J(\lambda,t)$ denotes transmembrane current. The task is to construct expressions for $I_{\rm P}$ and $I_{\rm D}$ that satisfy (5) for all constitutive forms for the current density $J(\lambda,t)$. The new approach to compartmental modelling requires a procedure or rule for partitioning transmembrane current between the proximal and distal boundaries of a segment. The rule used in this article is that transmembrane current flow to a boundary of a segment is proportional to the axial conductance of the segment lying between the point of application of the current and that boundary. If $G_{\rm P}(\lambda)$ is the axial conductance of the portion of segment lying between the point $\lambda$ and the proximal boundary of the segment, and $G_{\rm D}(\lambda)$ is the axial conductance of the portion of segment lying between the point $\lambda$ and the distal boundary of the segment, then

$$G_{\rm P}(\lambda) = \frac{\pi g_{\rm A} r_{\rm P} r(\lambda)}{\lambda h}\,, \qquad G_{\rm D}(\lambda) = \frac{\pi g_{\rm A} r_{\rm D} r(\lambda)}{(1-\lambda)h} \tag{6}$$

and the rule for partitioning transmembrane current leads to the expressions

$$\begin{aligned} I_{\rm P} &= h\int_0^1 \frac{G_{\rm P}J(\lambda,t)\,d\lambda}{G_{\rm P}+G_{\rm D}} = h\int_0^1 \frac{(1-\lambda)\,r_{\rm P}\,J(\lambda,t)\,d\lambda}{(1-\lambda)\,r_{\rm P}+\lambda\,r_{\rm D}}\,, \\ -I_{\rm D} &= h\int_0^1 \frac{G_{\rm D}J(\lambda,t)\,d\lambda}{G_{\rm P}+G_{\rm D}} = h\int_0^1 \frac{\lambda\,r_{\rm D}\,J(\lambda,t)\,d\lambda}{(1-\lambda)\,r_{\rm P}+\lambda\,r_{\rm D}}\,. \end{aligned} \tag{7}$$

Clearly these expressions satisfy identically condition (5) for the conservation of current.

### 3.3 Specification of transmembrane current

Transmembrane current is usually assumed to consist of four distinct components: capacitative current, intrinsic voltage-dependent current and point process input which is subdivided into synaptic current and exogenous point current. Total transmembrane current is represented by

$$\int 2\pi r\,c_{\rm M}\,\frac{\partial V}{\partial t}\,dx + \int 2\pi r\,J_{\rm IVDC}(V)\,dx + \sum J_{\rm SYN}(V_{\rm syn}) + \sum I_{\rm EX} \tag{8}$$

where the integrals and summations are taken over the length of a segment. In this expression $c_{\rm M}$ ($\mu$F/cm$^2$) is the specific capacitance of the segment membrane, $V(x,t)$ is the distribution of membrane potential at time $t$ (msec), $J_{\rm IVDC}(V)$ ($\mu$A/cm$^2$) is the density of transmembrane current due to intrinsic voltage-dependent channel activity, $J_{\rm SYN}(V_{\rm syn})$ ($\mu$A) describes synaptic input and $I_{\rm EX}$ ($\mu$A) describes exogenous input. Although the specific capacitance of dendritic membrane is normally taken to be constant in neuronal modelling, it will be treated here as a function of position to show how transmembrane current of this type may be incorporated into the new compartmental model. For a segment of length $h$, the expression for $J(\lambda,t)$ corresponding to formula (8) is

$$\begin{aligned} hJ(\lambda,t) &= 2\pi hr(\lambda)\,c_{\rm M}(\lambda)\,\frac{\partial V(\lambda,t)}{\partial t} + 2\pi hr(\lambda)\,J_{\rm IVDC}(V(\lambda,t)) \\ &\quad + \sum_k J_{\rm SYN}(V_{\rm syn})\,\delta(\lambda-\lambda_k) + \sum_k I_{\rm EX}(t)\,\delta(\lambda-\lambda_k) \end{aligned} \tag{9}$$

where $\lambda_k$ denotes the relative location of the $k^{th}$ synapse or exogenous input with respect to the proximal boundary of the segment ($\lambda = 0$).

## 4 The partitioning of transmembrane current

Further progress requires expressions for $I_{\rm P}$ and $I_{\rm D}$ in terms of the biophysical and morphological properties of the segment and the membrane potentials at its proximal and distal boundaries. Each component of the transmembrane current (9) is examined separately.

### 4.1 Point processes

We model synaptic current by the conventional constitutive equation $\mathcal{I} = g(t)(V-E)$ where $E$ is the reversal potential associated with the synapse and $g(t)$ is the time course of the synaptic

conductance. Exogenous point current input takes the form $\mathcal{I} = \mathcal{I}(t)$ where $\mathcal{I}(t)$ is a known function of $t$. Suppose that $\lambda_1, \cdots, \lambda_n$ are sites of point input $\mathcal{I}_1, \cdots \mathcal{I}_n$ to the segment, then it follows from expressions (7) that the contributions made to $I_{\rm P}$ and $I_{\rm D}$ from these currents are

$$I_{\rm P} = \sum_{k=1}^{n} \frac{r_{\rm P}}{r_k} (1 - \lambda_k) \mathcal{I}_k \,, \qquad -I_{\rm D} = \sum_{k=1}^{n} \frac{r_{\rm D}}{r_k} \lambda_k \mathcal{I}_k \tag{10}$$

where $r_k = (1 - \lambda_k) r_{\rm P} + \lambda_k r_{\rm D}$. In the special case of exogenous input alone, $\mathcal{I}_k = \mathcal{I}_k(t)$ and expressions (10) give the exact partitioning of this input. The procedure used by the anonymous reviewer (see Section 2.1) is an application of equations (10) to a uniform segment, that is,

$$I_{\rm P} = \sum_{k=1}^{n} (1 - \lambda_k) \mathcal{I}_k \,, \qquad -I_{\rm D} = \sum_{k=1}^{n} \lambda_k \mathcal{I}_k \,. \tag{11}$$

However, when synaptic input is present, expressions (10) for $I_{\rm P}$ and $I_{\rm D}$ will contain the (unknown) membrane potentials at the synapses, and its use will therefore require these potentials to be estimated in terms of known functions and the potentials at the proximal and distal boundaries of the segment.

One obvious way to estimate the potential at the site of a synapse is to use the potential distribution (4). However, the efficacy of this approximation relies on the validity of the assumption that transmembrane current is negligible by comparison with axial current. In the presence of synaptic input, transmembrane current need not be negligible by comparison with axial current, and so the partitioning rule must be developed to include this possibility.

## 4.2 The partitioning rule in the presence of synaptic input

The partitioning of point process input set out in Subsection 4.1 is developed by noting that this rule may be applied to the division of transmembrane current between nearest-neighbour sites of a point input, and that the proximal and distal boundaries of the segment are simply special cases of these sites. This application of the partitioning rule is equivalent to considering the balance between axial current and point current at each site of input ignoring the influence of distributed transmembrane current between sites. The implementation of the partitioning rule for general point process input is done in two stages. The first stage of the discussion focusses on the construction of the equations satisfied by the potentials at the sites of the point input, and the second stage of the discussion describes how these equations may be solved numerically and is contained in appendix one.

### 4.2.1 Equations for the potentials

In general, the locations of point process input can be taken to divide a segment into subsegments, defined to be the lengths of the segment between the locations of these inputs. Figure 2 is a schematic representation of a segment of length $h$ illustrating the relative locations

$\lambda_1, \cdots, \lambda_n$ of $n$ point inputs $\mathcal{I}_1, \cdots \mathcal{I}_n$ on a segment. Suppose axial current $I_k$ flows to the point $\lambda_k$ from the point $\lambda_{k-1}$ and that $V_k$ is the potential at the point $\lambda_k$.

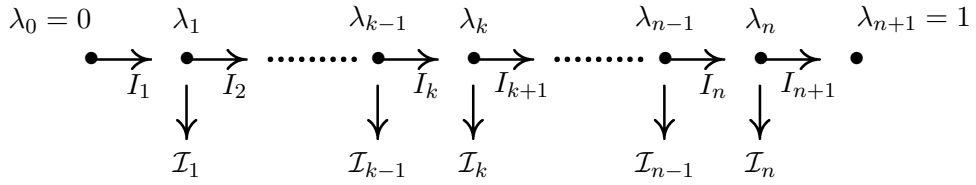


Figure 2: Configuration of point input to a dendritic segment of length $h$. Here $\mathcal{I}_k = g_k(t)(V_k - E_k)$ in the case of synaptic input at $\lambda_k$ or $\mathcal{I}_k = \mathcal{I}_k(t)$ if the input is an exogenous point current.

Since distributed current alone can flow across the membrane of a sub-segment, equation (3) may be used to describe the axial current in the $k$-th sub-segment by replacing $V_{\rm P}$ and $r_{\rm P}$ with $V_{k-1}$ and $r_{k-1}$ respectively, by replacing $V_{\rm D}$ and $r_{\rm D}$ with $V_k$ and $r_k$ respectively, and by replacing $h$ with $h(\lambda_k - \lambda_{k-1})$, the length of the sub-segment. If $V_1, \cdots, V_n$ are the potentials at the points $\lambda_1, \cdots, \lambda_n$ at which point process input is applied, then the axial currents $I_1, \cdots, I_{n+1}$ are related to the potentials $V_1, \cdots, V_n$ by the equations

$$I_k = \frac{\pi g_{\rm A} r_{k-1}\, r_k}{h(\lambda_k - \lambda_{k-1})}\,(V_{k-1} - V_k)\,, \qquad k = 1, \cdots, (n+1) \tag{12}$$

where it is understood that $\lambda_0 = 0$, $\lambda_{n+1} = 1$, $r_0 = r_{\rm P}$, $r_{n+1} = r_{\rm D}$, $V_0 = V_{\rm P}$ and $V_{n+1} = V_{\rm D}$. Equations (12) are rearranged in the form

$$V_{k-1} - V_k = \frac{h}{\pi g_{\rm A}}\,\frac{(\lambda_k - \lambda_{k-1})}{r_{k-1}\, r_k}\, I_k\,, \qquad k = 1, \cdots, (n+1)\,.$$

By recognising that $V_k - V_{\rm P}$ is the sum of the potential differences across the first $k$ sub-segments, it follows immediately from the previous equation that

$$V_k = V_{\rm P} - \frac{h}{\pi g_{\rm A}} \sum_{j=1}^{k} \frac{(\lambda_j - \lambda_{j-1})}{r_{j-1}\, r_j}\, I_j\,, \qquad k = 1, \cdots, n\,. \tag{13}$$

If $\lambda_k$ is the point of application of an exogenous input of strength $\mathcal{I}_k(t)$ then

$$I_{k+1} + \mathcal{I}_k(t) = I_k\,. \tag{14}$$

On the other hand, if there is a synapse at $\lambda_k$, then $\mathcal{I}_k = g_k(t)(V_k - E_k)$ and conservation of current requires that

$$I_{k+1} + g_k(V_k - E_k) = I_k\,. \tag{15}$$

Formula (13) for $V_k$ is now used to rewrite equation (15) in terms of axial currents to get

$$I_k - I_{k+1} + \frac{g_k h}{\pi g_{\rm A}} \sum_{j=1}^{k} \frac{(\lambda_j - \lambda_{j-1})}{r_{j-1}\, r_j}\, I_j = g_k(\, V_{\rm P} - E_k\,)\,, \qquad k = 1, \cdots, n\,. \tag{16}$$

Thus conservation of current at the points $\lambda_1, \cdots, \lambda_n$ gives rise to $n$ equations for the $(n+1)$ currents $I_1, \cdots, I_{n+1}$. In order to complete the system of equations specifying $I_1, \cdots, I_{n+1}$,

note that the potentials at the proximal and distal boundaries of the segment are known, and that this condition constrains the currents $I_1,\ \cdots,\ I_{n+1}$ to satisfy

$$\sum_{j=1}^{n+1} \frac{(\lambda_j - \lambda_{j-1}) r_{\rm P} r_{\rm D}}{r_{j-1}\, r_j}\, I_j = \frac{\pi g_{\rm A} r_{\rm P} r_{\rm D}}{h}\,(\,V_{\rm P} - V_{\rm D}\,)\,. \tag{17}$$

Equation (17) is obtained from equation (13) by asserting that $V_{n+1} = V_{\rm D}$. Note also that equation (17) has been multiplied by the factor $r_{\rm P} r_{\rm D}$ for the benefit of numerical work to make the coefficients of the currents in the rescaled equation order one. To summarise, the currents $I_1, \ldots I_{n+1}$ are determined by solving the linear equations

$$\left.\begin{aligned} I_k - I_{k+1} &= \mathcal{I}_k(t) \\ I_k - I_{k+1} + \frac{g_k h}{\pi g_{\rm A}} \sum_{j=1}^{k} \frac{(\lambda_j - \lambda_{j-1})}{r_{j-1}\, r_j}\, I_j &= g_k(\,V_{\rm P} - E_k\,)\,, \end{aligned}\right] \qquad k = 1, \cdots, n$$
$$\sum_{j=1}^{n+1} \frac{(\lambda_j - \lambda_{j-1}) r_{\rm P} r_{\rm D}}{r_{j-1}\, r_j}\, I_j = \frac{\pi g_{\rm A} r_{\rm P} r_{\rm D}}{h}\,(\,V_{\rm P} - V_{\rm D}\,) \tag{18}$$

where the first equation is used if $\lambda_k$ is the location of an exogenous point input and the second equation is used if $\lambda_k$ is the location of a synapse. The following example illustrates an application of equations (18) to the case of a single synapse and a single exogenous input.

**Example** Consider a segment which receives synaptic input of conductance $g_1(t)$ at $\lambda_1$ and exogenous current $\mathcal{I}_2(t)$ at $\lambda_2$ where $0 < \lambda_1 < \lambda_2 < 1$. This partitioning of the segment gives rise to three currents $I_1$, $I_2$ and $I_3$. The determination of $I_{\rm P}$ and $I_{\rm D}$ will require expressions for $I_1$ and $I_3$ in terms of the known conductance $g_1(t)$, the known current $\mathcal{I}_2(t)$, the geometry of the segment, and finally, the potentials $V_{\rm P}$ and $V_{\rm D}$ at the proximal and distal boundaries of the segment. The formulation of this problem will involve the current $I_2$ as an auxiliary variable, but the solution for $I_2$ is not sought. It follows from equations (18) that $I_1$, $I_2$ and $I_3$ satisfy

$$\begin{aligned} I_1 - I_2 + \frac{g_1(t) h}{\pi g_{\rm A}} \frac{(\lambda_1 - \lambda_0)}{r_0\, r_1}\, I_1 &= g_1(t)(\,V_{\rm P} - E_1\,)\,, \\ I_2 - I_3 &= \mathcal{I}_2(t)\,, \\ \frac{(\lambda_1 - \lambda_0) r_0\, r_3}{r_0\, r_1}\, I_1 + \frac{(\lambda_2 - \lambda_1) r_0\, r_3}{r_1\, r_2}\, I_2 + \frac{(\lambda_3 - \lambda_2) r_0\, r_3}{r_2\, r_3}\, I_3 &= \frac{\pi g_{\rm A} r_0\, r_3}{h}\,(\,V_{\rm P} - V_{\rm D}\,)\,. \end{aligned} \tag{19}$$

The first equation in (19) is equation (16) applied at the location of the synapse ($\lambda = \lambda_1$), and the second equation in (19) is equation (14) applied at the location of the exogenous current ($\lambda = \lambda_2$). The last equation in (19) is the the consistency condition expressed by equation (17). Equations (19) can be expressed in matrix form $AX = B$ where $X = [\,I_1, I_2, I_3\,]^{\rm T}$ and

$$A = \begin{bmatrix} 1 + \dfrac{g_1(t) h}{\pi g_{\rm A}} \dfrac{(\lambda_1 - \lambda_0)}{r_0\, r_1} & -1 & 0 \\ 0 & 1 & -1 \\ \dfrac{(\lambda_1 - \lambda_0) r_3}{r_1} & \dfrac{(\lambda_2 - \lambda_1) r_0\, r_3}{r_1\, r_2} & \dfrac{(\lambda_3 - \lambda_2) r_0}{r_2} \end{bmatrix}, \quad B = \begin{bmatrix} g_1(t)(V_{\rm P} - E_1) \\ \mathcal{I}_2(t) \\ \dfrac{\pi g_{\rm A} r_0\, r_3}{h}(V_{\rm P} - V_{\rm D}) \end{bmatrix}.$$

It is a matter of careful algebra to show that the currents $I_1$ and $I_3$ are given by the expressions

$$I_1 = \frac{\dfrac{\pi g_{\rm A} r_0\, r_3}{h}(V_{\rm P}-V_{\rm D}) + (1-\lambda_1)\dfrac{r_0}{r_1}g_1(t)(V_{\rm P}-E_1) + \mathcal{I}_2(t)(1-\lambda_2)\dfrac{r_0}{r_2}}{1+\dfrac{\lambda_1(1-\lambda_1)hg_1(t)}{\pi g_{\rm A} r_1^2}},$$

$$I_3 = \frac{\begin{array}{c}\dfrac{\pi g_{\rm A} r_0\, r_3}{h}\Big(1+\dfrac{\lambda_1 h g_1(t)}{\pi g_{\rm A} r_0 r_1}\Big)(V_{\rm P}-V_{\rm D}) - \dfrac{\lambda_1 r_3}{r_1}g_1(t)(V_{\rm P}-E_1) \\ - \mathcal{I}_2(t)\dfrac{r_3}{r_2}\Big(\lambda_2+\dfrac{\lambda_1(\lambda_2-\lambda_1)hg_1(t)}{\pi g_{\rm A} r_1^2}\Big)\end{array}}{1+\dfrac{\lambda_1(1-\lambda_1)hg_1(t)}{\pi g_{\rm A} r_1^2}}. \tag{20}$$

Of course, the complexity of these expressions for $I_1$ and $I_3$ is in part due to the fact that they combine the axial current in the segment in the absence of point input with the modification to this current due to the presence of the synaptic input at $\lambda=\lambda_1$ and the exogenous input at $\lambda=\lambda_2$. The perturbations $I_{\rm P}=I_1-I_{\rm PD}$ and $I_{\rm D}=I_3-I_{\rm PD}$ to the axial current at the proximal and distal boundaries of the segment are now calculated from formulae (3) and (20) to give

$$\begin{aligned} I_{\rm P} &= \frac{\dfrac{r_0(1-\lambda_1)}{r_1}\,g_1(t)(\,\psi_1-E_1\,)+\mathcal{I}_2(t)(1-\lambda_2)\dfrac{r_0}{r_2}}{1+\dfrac{\lambda_1(1-\lambda_1)hg_1(t)}{\pi g_{\rm A} r_1^2}}, \\ -I_{\rm D} &= \frac{\dfrac{\lambda_1 r_3}{r_1}\,g_1(t)(\,\psi_1-E_1\,)+\mathcal{I}_2(t)\dfrac{r_3}{r_2}\Big[\lambda_2+\dfrac{g_1(t)h\lambda_1(\lambda_2-\lambda_1)}{\pi g_{\rm A} r_1^2}\Big]}{1+\dfrac{\lambda_1(1-\lambda_1)hg_1(t)}{\pi g_{\rm A} r_1^2}}. \end{aligned} \tag{21}$$

where $\psi_1$ is the potential

$$\psi_1 = \frac{r_0(1-\lambda_1)V_{\rm P}+r_3\lambda_1 V_{\rm D}}{r_1}. \tag{22}$$

It is clear from (4) that $\psi_1$ would be the model potential at $\lambda=\lambda_1$ in the absence of transmembrane current, and therefore $g_1(t)(\,\psi_1-E_1\,)$ would be the transmembrane current supplied by the synapse at $\lambda=\lambda_1$ assuming that this synaptic current is negligible by comparison with the axial current. Furthermore, if the common denominator of expressions (21) is treated as unity, then expressions (21) simplify to

$$\begin{aligned} I_{\rm P} &= \frac{r_0(1-\lambda_1)}{r_1}\,g_1(t)(\,\psi_1-E_1\,)+\mathcal{I}_2(t)(1-\lambda_2)\frac{r_0}{r_2}, \\ -I_{\rm D} &= \frac{\lambda_1 r_3}{r_1}\,g_1(t)(\,\psi_1-E_1\,)+\mathcal{I}_2(t)\frac{r_3}{r_2}\,\lambda_2, \end{aligned} \tag{23}$$

which are identical to equations (10) with $\mathcal{I}_1=g_1(t)(\,\psi_1-E_1\,)$ and $\mathcal{I}_2=\mathcal{I}(t)$. Expressions (23) are those that would follow from making the assumption that transmembrane current is negligible by comparison with axial current in the presence of synaptic input. Consequently, the use of expressions (23) for $I_{\rm P}$ and $I_{\rm D}$ would overestimate the true strength of both the synaptic

and the exogenous input to a segment. In conclusion, synaptic and exogenous input do not act independently when a segment receives both types of point process input.

The second stage of the analysis deals with the construction and numerical solution of the equations constructed from the particular configuration of synapses and exogenous input, and is given in Appendix 1.

## 4.3 Distributed transmembrane current

All distributed transmembrane current is treated using equations (7) with appropriate expressions for $J(\lambda, t)$, and with occurrences of the membrane potential approximated by expression (4). Capacitative current and intrinsic voltage-dependent current are considered separately.

### 4.3.1 Capacitative transmembrane current

The component of capacitative current in (9) is estimated by approximating the true membrane potential along the segment by expression (4) to obtain

$$J^{\,\mathrm{cap}}(\lambda,t) = 2\pi c_{\mathrm{M}}(\lambda) r(\lambda) \frac{dV(\lambda,t)}{dt} = 2\pi c_{\mathrm{M}}(\lambda) \Big[\, (1-\lambda)\, r_{\mathrm{P}}\, \frac{dV_{\mathrm{P}}}{dt} + \lambda\, r_{\mathrm{D}} \frac{dV_{\mathrm{D}}}{dt} \,\Big]. \tag{24}$$

It now follows from expressions (7) that the contributions made by capacitative transmembrane current to $I_{\mathrm{P}}$ and to $I_{\mathrm{D}}$ are

$$\begin{aligned} I_{\mathrm{P}}^{\mathrm{cap}} &= 2\pi\, r_{\mathrm{P}} h \Big[ r_{\mathrm{P}} \frac{dV_{\mathrm{P}}}{dt} \int_0^1 \frac{(1-\lambda)^2 c_{\mathrm{M}}(\lambda)\, d\lambda}{(1-\lambda)\, r_{\mathrm{P}} + \lambda\, r_{\mathrm{D}}} + r_{\mathrm{D}} \frac{dV_{\mathrm{D}}}{dt} \int_0^1 \frac{\lambda(1-\lambda) c_{\mathrm{M}}(\lambda)\, d\lambda}{(1-\lambda)\, r_{\mathrm{P}} + \lambda\, r_{\mathrm{D}}} \Big], \\ -I_{\mathrm{D}}^{\mathrm{cap}} &= 2\pi\, r_{\mathrm{D}} h \Big[ r_{\mathrm{P}} \frac{dV_{\mathrm{P}}}{dt} \int_0^1 \frac{\lambda(1-\lambda) c_{\mathrm{M}}(\lambda)\, d\lambda}{(1-\lambda)\, r_{\mathrm{P}} + \lambda\, r_{\mathrm{D}}} + r_{\mathrm{D}} \frac{dV_{\mathrm{D}}}{dt} \int_0^1 \frac{\lambda^2 c_{\mathrm{M}}(\lambda)\, d\lambda}{(1-\lambda)\, r_{\mathrm{P}} + \lambda\, r_{\mathrm{D}}} \Big]. \end{aligned} \tag{25}$$

If the compartment is a uniform cylinder with constant specific membrane capacitance, the perturbations in axial current at the proximal and distal boundaries of the segment may be computed by evaluating the integrals in formulae (25) to get

$$I_{\mathrm{P}}^{\mathrm{cap}} = \frac{C}{6} \Big[\, 2\frac{dV_{\mathrm{P}}}{dt} + \frac{dV_{\mathrm{D}}}{dt} \,\Big], \qquad -I_{\mathrm{D}}^{\mathrm{cap}} = \frac{C}{6} \Big[\, \frac{dV_{\mathrm{P}}}{dt} + 2\frac{dV_{\mathrm{D}}}{dt} \,\Big] \tag{26}$$

where $C$ is the total membrane capacitance of the segment. The calculation for tapered segments with non-uniform membrane specific capacitance is presented in Appendix 2.

### 4.3.2 Intrinsic voltage-dependent transmembrane current

The construction of $I_{\mathrm{P}}^{\mathrm{cap}}$ and $I_{\mathrm{D}}^{\mathrm{cap}}$ for a membrane with non-constant specific capacitance provides the framework for treating intrinsic voltage-dependent transmembrane current. For an ionic species $\alpha$, this current is usually described by the constitutive formula $J = g_\alpha(\boldsymbol{\theta})(V - E_\alpha)$ where $V$ is the membrane potential, $E_\alpha$ is the reversal potential for species $\alpha$ and $g_\alpha(\boldsymbol{\theta})$ is a membrane conductance which depends on a set of auxiliary variables $\boldsymbol{\theta}$, for example, the probabilities $m$, $n$ and $h$ appearing in the Hodgkin-Huxley (1952) model.

In the case of a *passive* membrane, the conductance $g_\alpha(\boldsymbol{\theta})$ takes a constant (but different) value for each species. The total transmembrane current density is obtained by summing the transmembrane current densities of each ionic species to get

$$J = \sum_\alpha g_\alpha(V - E_\alpha) = g_{\rm M}(V - E)\,, \qquad g_{\rm M} = \sum_\alpha g_\alpha\,, \quad E = \sum_\alpha \frac{g_\alpha}{g_{\rm M}}\, E_\alpha\,. \tag{27}$$

Thus the constitutive equation for the transmembrane current density of a passive membrane is $J = g_{\rm M}(V - E)$ where $g_{\rm M}$ (mS/cm$^2$) is the total membrane conductance and $E$ plays the role of a reversal potential. When the segment is a uniform cylinder with a membrane of constant conductance, the contributions to $I_{\rm P}$ and $I_{\rm D}$ mimic formulae (26) for capacitative current and are respectively

$$I_{\rm P}^{\rm IVDC} = \frac{G}{6}\Big[2(V_{\rm P} - E) + (V_{\rm D} - E)\Big]\,, \qquad -I_{\rm D}^{\rm IVDC} = \frac{G}{6}\Big[(V_{\rm P} - E) + 2(V_{\rm D} - E)\Big] \tag{28}$$

where $G$ is the total membrane conductance of the segment. The treatment of tapered segments with non-uniform membrane conductance is presented in Appendix 3.

# 5 Comparison of the traditional and new approaches to compartmental modelling

Two simulation studies are used to compare the performance of the traditional and new compartmental models. These studies are based on a branched model neuron with known expression for the somal potential in response to large scale exogenous input (see Appendix 4). The first study examines the accuracy with which each type of compartmental model estimates this somal potential, and uses the NEURON simulator (Hines and Carnevale, 1997) as an example of a traditional compartmental model. The second study assesses the accuracy of the two types of models by comparing the statistics of the spike train output generated by each model when the test neuron is subjected to large scale synaptic input. Here a traditional compartmental model developed by the authors is used. This model gave results identical to those of NEURON in the first study. Finally, a time step of one microsecond is used in the numerical integration of each compartmental model to ensure that errors in temporal integration make no significant contribution to the error in the calculation of membrane potential.

## 5.1 The test neuron

One way to construct a branched test neuron with a closed form solution for the somal potential is to choose the radii and lengths of its sections such that the Rall conditions for an equivalent cylinder are satisfied (Rall, 1964). These conditions require that the sum of the three-halves power of the diameters of the child limbs is equal to the three-halves power of the diameter of the parent limb at any branch point, and that the total electrotonic length from a branch point or the soma to a dendritic tip is independent of path. The test neuron illustrated in Figure 3

satisfies these conditions. When the Rall conditions are satisfied, the effect at the soma of any configuration of input on the branched model of the neuron is identical to the effect at the soma of the unbranched equivalent cylinder with biophysical properties and configuration of input determined uniquely from those of the original branched neuron (Lindsay *et al.*, 2003).

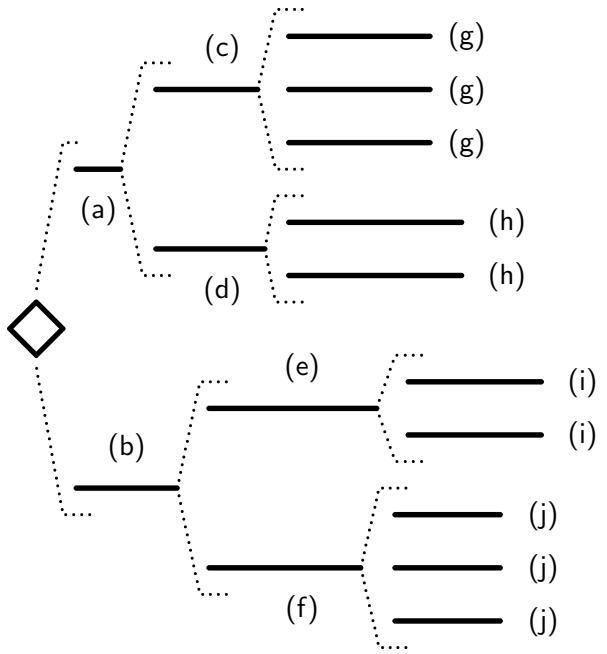


| Section | Length $\mu$m | Diameter $\mu$m |
|---|---|---|
| $(a)$ | 166.809245 | 7.089751 |
| $(b)$ | 379.828386 | 9.189790 |
| $(c)$ | 383.337494 | 4.160168 |
| $(d)$ | 410.137845 | 4.762203 |
| $(e)$ | 631.448520 | 6.345604 |
| $(f)$ | 571.445800 | 5.200210 |
| $(g)$ | 531.582750 | 2.000000 |
| $(h)$ | 651.053246 | 3.000000 |
| $(i)$ | 501.181023 | 4.000000 |
| $(j)$ | 396.218388 | 2.500000 |

Figure 3: A branched neuron satisfying the Rall conditions. The diameters and lengths of the dendritic sections are given in the right hand panel of the figure. At each branch point, the ratio of the length of a section to the square root of its radius is fixed for all children of the branch point.

The high degree of accuracy used in the specification of the dendritic radii and section lengths of the test neuron is required to ensure that the equivalent cylinder is an adequate representation of the test neuron. The membrane of the test neuron is assigned a specific conductance of $0.091\,\mathrm{mS/cm^2}$ ($g_\mathrm{M}$) and specific capacitance of $1.0\,\mu\mathrm{F/cm^2}$ ($c_\mathrm{M}$), and has axoplasm of conductance $14.286\,\mathrm{mS/cm}$ ($g_\mathrm{A}$). With these biophysical properties, the equivalent cylinder has length one electrotonic unit. The soma of the test neuron is assumed to have membrane area $A_\mathrm{S}$, and specific conductance $g_\mathrm{S}$ and specific capacitance $c_\mathrm{S}$ identical to that of the dendritic membrane. The analytical expression for its somal potential is given in Appendix 4.

## 5.2 First simulation study

In this study, the performance of a traditional and the new compartmental model is compared by assessing the accuracy with which both models determine the time course of the somal potential of the test neuron (Figure 3) when the neuron is subjected to large scale exogenous

point input. Each simulation distributes 75 point inputs at random over the dendritic tree of the test neuron, where each input has strength $2 \times 10^{-5}\,\mu$A. These inputs are then mapped to positions on the Rall equivalent cylinder at the same electrotonic distance from the soma (assumed to be a sphere of diameter $40\,\mu$m). The time course of the potential at the soma of the equivalent cylinder due to the combined effect of these inputs is determined analytically and taken to be the reference potential against which error in both compartmental models is measured. The difference between a computed potential and its exact value is determined at one millisecond intervals in the first 10 milliseconds of the simulation, and each difference is divided by the exact potential at that time to get a relative measure of error. The simulation procedure is repeated 2000 times to determine the statistics of the relative error for each of 13 different levels of spatial discretisation (number of compartments).

### 5.2.1 Results

The results for this study are set out in Table 2. This table shows the common logarithms of the mean value of the modulus of the relative error and the standard deviation of that error estimated ten milliseconds after the initiation of the stimulus. Similar results (not shown) hold for all times at which the errors were estimated.

| Compartments ($\log_{10}$(Compartments)) | | Traditional | New Model | Traditional | New Model |
|---|---|---|---|---|---|
| | | $\log_{10}$(Mean) | | $\log_{10}$(Standard Dev.) | |
| 17 | (1.2305) | −2.41151 | −2.71945 | −2.62290 | −3.19338 |
| 21 | (1.3222) | −2.47233 | −2.77674 | −2.69851 | −3.24583 |
| 34 | (1.5314) | −2.94299 | −3.41196 | −3.06731 | −3.88820 |
| 41 | (1.6127) | −3.04729 | −3.62138 | −3.17081 | −4.14997 |
| 54 | (1.7323) | −3.21258 | −3.89150 | −3.34889 | −4.41251 |
| 61 | (1.7853) | −3.24692 | −3.91268 | −3.37653 | −4.45051 |
| 75 | (1.8750) | −3.35180 | −4.12056 | −3.46881 | −4.65463 |
| 82 | (1.9138) | −3.39846 | −4.23567 | −3.51591 | −4.76498 |
| 93 | (1.9684) | −3.45602 | −4.30636 | −3.57633 | −4.82045 |
| 193 | (2.2855) | −3.77417 | −4.94731 | −3.89829 | −5.47886 |
| 293 | (2.4668) | −3.94409 | −5.31876 | −4.07811 | −5.84771 |
| 390 | (2.5910) | −4.08234 | −5.57349 | −4.20025 | −6.10791 |
| 495 | (2.6946) | −4.15996 | −5.78252 | −4.28525 | −6.32790 |

Table 2: The result of 2000 simulations for each of 13 different levels of discretisation used in the implementation of a traditional and new compartmental model. The common logarithms of the mean value of the modulus of the relative error and the standard deviation of that error are estimated at ten milliseconds after the initiation of the stimulus.

The left hand panel of Figure 4 shows regression lines of the common logarithms of the modulus of the mean relative error (denoted by $\overline{RE}$ ) for the traditional (dashed line) and new (solid line) compartmental models on the logarithm of the number of compartments (denoted by $N$) used to represent the model neuron. These lines, based on the data in Table 2, have equations

$$\begin{aligned} \log_{10} \overline{RE}_{\text{traditional}} &= -1.09 - 1.17 \log_{10} N \,, \\ \log_{10} \overline{RE}_{\text{new}} &= -0.17 - 2.10 \log_{10} N \end{aligned} \tag{29}$$

in which the regressions are achieved with adjusted $R^2$ values[2] of 97.4% and 99.5% respectively. In view of the very high $R^2$ values for these regression equations, a number of conclusions can be drawn from this simulation study. For a fixed number of compartments, the error in the new compartmental model is always less than that of the traditional model. The regression equations (29) support the argument made in Section 2.1 that the error in a traditional compartmental model in the presence of exogenous point current input is approximately $O(1/n)$, whereas the comparable error in the new compartmental model is approximately $O(1/n^2)$. In practical terms, for example, the regression results (29) suggest that the new compartmental model with 100 compartments achieves approximately the same level of accuracy as a traditional model with 500 compartments.

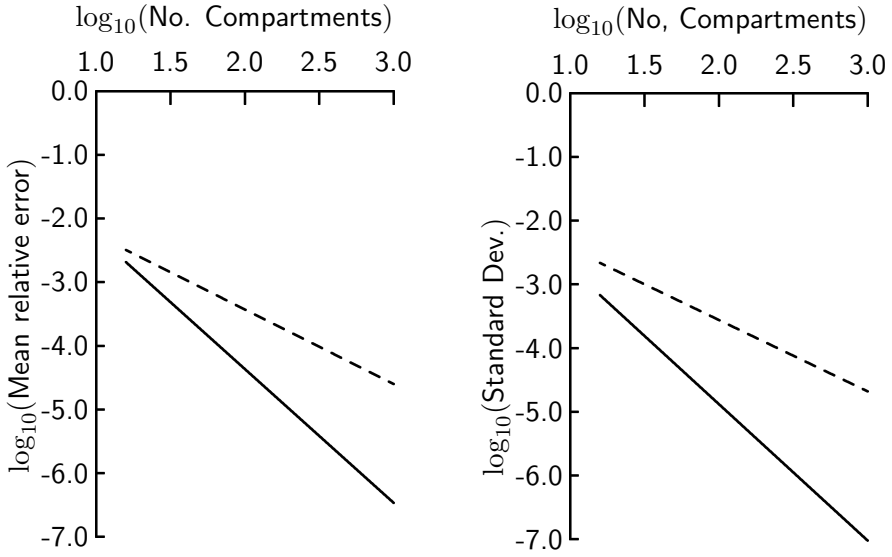


Figure 4: The left panel shows the regression lines of the common logarithm of the mean relative errors in the new compartmental model (solid line) and a traditional compartmental model (dashed line) against the common logarithm of the number of compartments. All errors are measured ten milliseconds after initiation of the stimulus. The right panel shows the regression lines for the standard deviations of the mean relative errors for the new compartmental model (solid line) and for a traditional compartmental model (dashed line).

[2] $R^2$ measures the proportion of the total variation of the dependent variable about its mean value that is explained by the regression, and necessarily takes a value between zero and one expressed as a percentage.

The standard deviation (SD) of the modulus of the relative error can be regarded as an indicator of the reliability of a single application of the model. The right hand panel of Figure 4 shows regression lines of the common logarithms of the standard deviation of the modulus of the relative error for the traditional (dashed line) and new (solid line) compartmental models on the logarithm of the number of compartments used to represent the model neuron. These lines, based on the data in Table 2, have equations

$$\begin{aligned} \log_{10} \mathrm{SD}_{\mathrm{traditional}} &= -1.32 - 1.12 \log_{10} N \,, \\ \log_{10} \mathrm{SD}_{\mathrm{new}} &= -0.60 - 2.14 \log_{10} N \end{aligned} \tag{30}$$

in which the regressions are achieved with adjusted $R^2$ values of 98.7% and 99.4% respectively. These regression lines show that the new compartmental model is more reliable than a traditional compartmental model. For example, a traditional compartmental model requires at least 100 compartments to give a standard deviation of the modulus of the relative error that is smaller than that of the new compartmental model using 40 compartments.

### 5.3 Second simulation study

In the second simulation study 100 synapses are distributed at random over the dendritic tree of the test neuron illustrated in Figure 3. Each synapse is activated independently of all other synapses, has a maximum conductance of $3 \times 10^{-5}$ mS and a rise time of 0.5 msec. Activation times for each synapse follow Poisson statistics with a mean rate of 30 pre-synaptic spikes per second. Spikes are generated by the soma of the test neuron using Hodgkin-Huxley kinetics. This study is based on 12 different levels of spatial discretisation (number of compartments) in which each simulation of the traditional and new compartmental models use identical synaptic firing times and identical numbers of compartments.

#### 5.3.1 Results

Table 5 gives the spike rate of soma-generated action potentials based on 11 seconds of activity, the first second of which is ignored.

Figure 5 illustrates the data set out in Table 3 in which the spike rates for the traditional model (dashed line) and new model (solid line) are plotted against the common logarithm of $N$, the number of compartments used in each simulation. As $N$ is increased, the spike rates generated by both models approach a common limit. However, the spike rate generated by the traditional model approaches this limit more slowly and appears to oscillate as the limit is approached. The spike rate obtained using the traditional model with 500 compartments is achieved in the new model with only 100 compartments. These differences in the number of compartments required to achieve the same level of accuracy in both models are identical to those observed in the first study.

| Compartments ($\log_{10}$(Compartments)) | Traditional Model Mean Firing Rate | New Model Mean Firing Rate |
|---|---|---|
| 34 (1.5314) | 31.5 | 27.6 |
| 41 (1.6127) | 30.3 | 27.9 |
| 54 (1.7323) | 30.5 | 27.5 |
| 61 (1.7853) | 29.8 | 27.2 |
| 75 (1.8750) | 29.2 | 27.0 |
| 82 (1.9138) | 28.5 | 27.0 |
| 93 (1.9684) | 28.3 | 26.8 |
| 193 (2.2855) | 26.5 | 26.5 |
| 293 (2.4668) | 25.9 | 26.2 |
| 390 (2.5910) | 26.2 | 26.2 |
| 495 (2.6946) | 26.7 | 26.2 |
| 992 (2.9965) | 26.0 | 26.1 |

Table 3: The spike rate estimated from a 10 second record of spike train activity obtained from a traditional and the new compartmental model at 12 different levels of spatial discretisation (number of compartments).

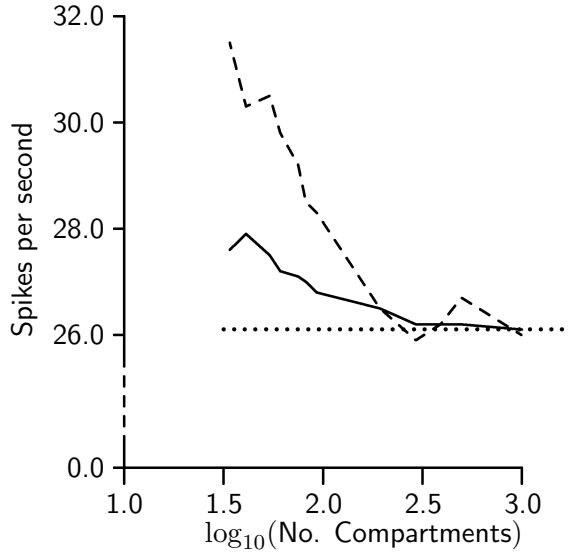


Figure 5: The spike rate plotted against the common logarithm of the number of compartments for a traditional compartmental model (dashed line) and the new compartmental model (solid line). The dotted line shows the expected spike rate.

### 5.3.2 Comparison of model-generated spike trains

It is clear from Figure 5 that the mean rate of the spike train generated by the new compartmental model converges more quickly to the theoretical mean spike rate than that generated

by a traditional compartmental model. One would therefore infer from the behaviour of this summary statistic that the spike train generated by the former is a more accurate representation of the spiking behaviour of the test neuron in response to synaptic activity than that generated by the latter. To investigate the validity of this inference requires an accurate comparison of the times of occurrence of the spikes in the spike trains generated by each model with identical synaptic activity applied to the test neuron. We take as our reference the times of occurrence of the spikes generated in ten seconds using the new compartmental model with 100 compartments (spike train $\mathcal{N}_{100}$). These spike times are compared with those generated by a traditional compartmental model with 100 compartments and with 500 compartments[3] (spike trains $\mathcal{T}_{100}$ and $\mathcal{T}_{500}$ respectively). The times of occurrence of spikes in the spike trains to be compared are taken to be identical if they occur within one millisecond of each other. The comparison between $\mathcal{N}_{100}$ and $\mathcal{T}_{100}$ revealed 244 spikes common to both spike trains (*i.e.* occurring within one millisecond of each other). There were 24 spikes unique to $\mathcal{N}_{100}$ and 39 spikes unique to $\mathcal{T}_{100}$. The comparison between $\mathcal{N}_{100}$ and $\mathcal{T}_{500}$ revealed 258 spikes common to both spike trains with 10 spikes unique to $\mathcal{N}_{100}$ and 9 spikes unique to $\mathcal{T}_{500}$. Since the reference spike train $\mathcal{N}_{100}$ is common to both comparisons, it is clear that as the number of compartments in a traditional model increases, the spike train generated by that model will conform more closely to that generated by the new compartmental model with significantly fewer compartments.

## 6 Concluding remarks

We have demonstrated that it is possible to achieve a significant increase in the accuracy and precision of compartmental models by developing a new compartmental model in which compartments have two potentials – one at either end of the segment which the compartment represents. The new compartment acts as fundamental unit in the construction of a model of a branched dendrite. When these compartments are connected by requiring continuity of potential and conservation of current at segment boundaries, they provide a new type of compartmental model with a mathematical form identical to that of a traditional model in the sense that both types of compartmental model involve only nearest neighbour interactions. One demonstrated benefit of the new compartmental model is that it provides a mechanism to take account of the exact location of point process input by contrast with traditional compartmental models which would assign this input to an accuracy of half the length of a segment. We would anticipate that the application of the new compartmental model would be most useful in association with experiments in which the precise timing of spikes is thought to be important (*e.g.*, Oram *et al.*, 1999 and the references therein) or in studies investigating the influence of the location of synaptic input on the mean rate of the spike train output (*e.g.*, Poirazi *et al.*, 2003).

[3]All the simulations were run on a PC with dual Athlon 1500MP processors. The times required to simulate 10 seconds of spike train data were 61 minutes for the new compartmental model with 100 compartments, 41 minutes and 353 minutes for a traditional compartmental model with 100 and 500 compartments respectively. In the presence of point current input alone, the computational times for both models are identical.

## Acknowledgement

A.E. Lindsay would like to thank the Wellcome Trust for the award of Vacation Scholarship (VS/03/GLA/8/SL/TH/FH).

## References

Bower JM and Beeman D (1997) The book of GENESIS. 2nd ed. NY Telos.

Hines M and Carnevale N (1997) The NEURON simulation environmment. *Neural Computation* 9:1179-1209.

Hodgkin AL and Huxley AF (1952) A quantitative description of membrane current and its application to conduction and excitation in nerve. *Journal of Physiology* 117:500-544.

Lindsay KA, Rosenberg JR and Tucker G (2003). Analytical and numerical construction of equivalent cables. *Mathematical Biosciences* 184:137-164.

Oram MW, Wiener MC, Lestienne R, Richmond BJ (1999) Stochastic nature of precisely timed spike patterns in visual system neuronal responses. *Journal of Neurophysiology* 81:3021-3033.

Poriazi P, Brannon T, and Mel BW (2003). Pyramidal neuron as two-layer neural network *Neuron* 37:989-999.

Rall W (1964) Theoretical significance of dendritic trees and motoneuron input-output relations. In *Neural Theory and Modelling.* R.F.Reiss (ed.). Stanford University Press, Stanford CA.

Segev I and Burke RE (1998) Compartmental models of complex neurons. In *Methods in Neuronal Modeling - from ions to networks* 2nd Edition. Koch C and Segev I (eds.). Ch.3, pp 93-136. MIT Press, MA.

**Appendix 1 – Numerical estimation of perturbations to axial current**

The example in Subsection 4.2 demonstrates that synaptic and exogenous input do not act independently. This means that both types of point process input must be treated simultaneously in the construction of the equations to determine the perturbations $I_{\rm P}$ and $I_{\rm D}$ of the axial current. The equations for the perturbations in axial current are constructed by replacing $I_k$ in equations (14, 16 and 17) by $I_{\rm PD} + \widehat{I}_k$ where $\widehat{I}_k$ is the perturbation to $I_k$. If $\lambda = \lambda_k$ is the site of an exogenous input then the appropriate equation for the perturbed currents is

$$\widehat{I}_k - \widehat{I}_{k+1} = \mathcal{I}_k(t)\,, \tag{31}$$

whereas if $\lambda = \lambda_k$ is the site of a synapse with conductance $g_k(t)$, the appropriate equation is

$$\widehat{I}_k - \widehat{I}_{k+1} + \frac{g_k h}{\pi g_{\rm A}} \sum_{j=1}^{k} \frac{(\lambda_j - \lambda_{j-1})}{r_{j-1}\, r_j}\, \widehat{I}_j = \mathcal{I}_k(t) \tag{32}$$

where the current $\mathcal{I}_k(t)$ is defined by the formula

$$\mathcal{I}_k(t) = g_k(t) \left[ (1-\lambda_k) \frac{r_{\rm P}}{r_k}\, V_{\rm P} + \lambda_k \frac{r_{\rm D}}{r_k}\, V_{\rm D} - E_k \right]. \tag{33}$$

The derivation of equation (32) takes advantage of the identity

$$\sum_{j=1}^{k} \frac{(\lambda_j - \lambda_{j-1})}{r_{j-1}\, r_j} = \frac{\lambda_k}{r_{\rm P}\, r_k}\,,$$

which can be established by induction. Note that expression (33) for $\mathcal{I}_k(t)$ when $\lambda = \lambda_k$ is a synapse is precisely the current that would be expected to flow at the synapse if the distribution of potential on the segment was described by expression (4). Finally, equation (17) simplifies to

$$\sum_{j=1}^{n+1} \frac{(\lambda_j - \lambda_{j-1}) r_{\rm P}\, r_{\rm D}}{r_{j-1}\, r_j}\, \widehat{I}_j = 0 \tag{34}$$

where the constant multiplier $r_{\rm P}\, r_{\rm D}$ has been added without loss to make the coefficients of this equation comparable to those appearing in the first $n$ equations. Equations (31,32 and 34) may be represented compactly in matrix notation by

$$A\,\widehat{I} + GC\,\widehat{I} = \mathcal{I} \tag{35}$$

where $\widehat{I} = [\widehat{I}_1,\ \cdots\ , \widehat{I}_{n+1}]^{\rm T}$ is the $(n+1)$ dimensional column vector of perturbations in axial current, $\mathcal{I} = [\mathcal{I}_1,\ \cdots\ , \mathcal{I}_n, 0\,]^{\rm T}$ and $A$ is the $(n+1) \times (n+1)$ matrix

$$\begin{bmatrix} 1 & -1 & 0 & \cdots & \cdots & 0 \\ 0 & 1 & -1 & \cdots & \cdots & 0 \\ 0 & 0 & 1 & \cdots & \cdots & 0 \\ \cdots & \cdots & \cdots & \cdots & \cdots & \cdots \\ 0 & 0 & 0 & \cdots & 1 & -1 \\ \dfrac{\lambda_1 r_{\rm P} r_{\rm D}}{r_0 r_1} & \dfrac{(\lambda_2 - \lambda_1) r_{\rm P} r_{\rm D}}{r_1 r_2} & \dfrac{(\lambda_3 - \lambda_2) r_{\rm P} r_{\rm D}}{r_2 r_3} & \cdots & \dfrac{(\lambda_n - \lambda_{n-1}) r_{\rm P} r_{\rm D}}{r_{n-1} r_n} & \dfrac{(1 - \lambda_n) r_{\rm P} r_{\rm D}}{r_n r_{n+1}} \end{bmatrix}. \tag{36}$$

Briefly, $G$ is an $(n+1)\times(n+1)$ diagonal matrix in which the $(k,k)$ entry is zero if $\lambda_k$ is the site of an exogenous input and takes the value $g_k(t)$ if $\lambda_k$ is the site of a synapse. The $(n+1,n+1)$ entry of $G$ is always zero. The matrix $C$ is a lower triangular matrix of type $(n+1)\times(n+1)$ in which all the nonzero entries in the $k^{th}$ column take the value $(\lambda_k-\lambda_{k-1})/(\pi g_{\rm A} r_{k-1}\, r_k)$.

**Multiple point inputs**

To take account of the influence of the matrix $GC$ in the solution of equation (35), the algorithm

$$A\widehat{I}^{(m+1)} = \mathcal{I} - GC\widehat{I}^{(m)} \tag{37}$$

is iterated with initial condition $A\widehat{I}^{(0)} = \mathcal{I}$. Although it can be demonstrated that the matrix $A$ has a simple closed form expression for its inverse, it is not (numerically) efficient to use this expression to solve equation (37). Instead, we observe that $A$ has an $LU$ factorisation in which $U$ is the $(n+1)\times(n+1)$ upper triangular matrix with ones everywhere in the main diagonal, negative ones everywhere in the super-diagonal and zero everywhere else, and $L$ is the $(n+1)\times(n+1)$ lower triangular matrix

$$\begin{bmatrix} 1 & 0 & 0 & 0 & \cdots & \cdots & 0 \\ 0 & 1 & 0 & 0 & \cdots & \cdots & 0 \\ 0 & 0 & 1 & 0 & \cdots & \cdots & 0 \\ \cdots & \cdots & \cdots & \cdots & \cdots & \cdots & \cdots \\ \dfrac{\lambda_1\, r_{\rm P}}{r_1} & \dfrac{\lambda_2\, r_{\rm P}}{r_2} & \dfrac{\lambda_3\, r_{\rm P}}{r_3} & \dfrac{\lambda_4\, r_{\rm P}}{r_4} & \cdots & \dfrac{\lambda_n\, r_{\rm P}}{r_n} & 1 \end{bmatrix}. \tag{38}$$

Since $\mathcal{I}$ is a linear combination of $V_{\rm P}$, $V_{\rm D}$ and a voltage independent term, then the solution to equation (37) has general representation

$$\widehat{I} = \phi_1(t)V_{\rm P} + \phi_2(t)V_{\rm D} + \phi_3(t) \tag{39}$$

where $\phi_1(t)$, $\phi_2(t)$ and $\phi_3(t)$ satisfy

$$\begin{aligned} A\,\phi_1 &= \Big[g_1(1-\lambda_1)\frac{r_{\rm P}}{r_1},\ \cdots\ ,\ g_n(1-\lambda_n)\frac{r_{\rm P}}{r_n}, 0\Big]^{\rm T} - GC\,\phi_1\,, \\ A\,\phi_2 &= \Big[g_1\lambda_1\frac{r_{\rm D}}{r_1},\ \cdots\ ,\ g_n\lambda_n\frac{r_{\rm D}}{r_n}, 0\Big]^{\rm T} - GC\,\phi_2\,, \\ A\,\phi_3 &= -\Big[g_1E_1,\ \cdots\ ,\ g_nE_n, 0\Big]^{\rm T} - GC\,\phi_3\,. \end{aligned} \tag{40}$$

The equations (40) for $\phi_1(t)$, $\phi_2(t)$ and $\phi_3(t)$ may be solved easily by an iterative procedure based on the sparse $LU$ factorisation of $A$. If the conductances $g_1,\ \cdots,\ g_n$ are sufficiently small, the solution of equations (40) is well approximated by ignoring the second term on the right hand side or equations (40). This approximation is equivalent to using the partitioning rule (7) in combination with formula (4) for the membrane potential.

**Special case of exogenous input**

If $\lambda_1,\ \cdots\ ,\lambda_n$ are sites of exogenous input $\mathcal{I}_1,\ \cdots \mathcal{I}_n$ then $G = 0$ in equation (37) and $\mathcal{I}$ is the vector of exogenous currents. In this case, expressions (10) for $I_{\rm P}$ and $I_{\rm D}$ are obtained immediately as the first and last entries in the solution $\widehat{I}$ of equation $A\,\widehat{I} = LU\,\widehat{I} = \mathcal{I}$.

**Appendix 2 – The partitioning of capacitative current on tapered cylinders**

Recall from expressions (7) that the contributions made to the proximal and distal perturbations to the axial current as a consequence of capacitative transmembrane current on a tapered segment with membrane of variable specific capacitance are respectively

$$\begin{aligned} I_{\rm P}^{\rm cap} &= 2\pi\, r_{\rm P} h\Big[r_{\rm P}\frac{dV_{\rm P}}{dt}\int_0^1 \frac{(1-\lambda)^2 c_{\rm M}(\lambda)\,d\lambda}{(1-\lambda)\,r_{\rm P}+\lambda\,r_{\rm D}} + r_{\rm D}\frac{dV_{\rm D}}{dt}\int_0^1 \frac{\lambda(1-\lambda)c_{\rm M}(\lambda)\,d\lambda}{(1-\lambda)\,r_{\rm P}+\lambda\,r_{\rm D}}\Big], \\ -I_{\rm D}^{\rm cap} &= 2\pi\, r_{\rm D} h\Big[r_{\rm P}\frac{dV_{\rm P}}{dt}\int_0^1 \frac{\lambda(1-\lambda)c_{\rm M}(\lambda)\,d\lambda}{(1-\lambda)\,r_{\rm P}+\lambda\,r_{\rm D}} + r_{\rm D}\frac{dV_{\rm D}}{dt}\int_0^1 \frac{\lambda^2 c_{\rm M}(\lambda)\,d\lambda}{(1-\lambda)\,r_{\rm P}+\lambda\,r_{\rm D}}\Big]. \end{aligned} \tag{41}$$

For tapered segments ($r_{\rm P} \neq r_{\rm D}$) with membranes of non-uniform specific capacitance, the integrals in (41) have values

$$\begin{aligned} I_{\rm P}^{\rm cap} &= 2\pi h\, r_{\rm P}\Big[c_{\rm P}\psi(r_{\rm P},r_{\rm D}) + c_{\rm D}\phi(r_{\rm P},r_{\rm D})\Big]\frac{dV_{\rm P}}{dt} \\ &\qquad + 2\pi h\Big[c_{\rm P} r_{\rm D}\phi(r_{\rm P},r_{\rm D}) + c_{\rm D} r_{\rm P}\phi(r_{\rm D},r_{\rm P})\Big]\frac{dV_{\rm D}}{dt}, \\ -I_{\rm D}^{\rm cap} &= 2\pi h\Big[c_{\rm P} r_{\rm D}\phi(r_{\rm P},r_{\rm D}) + c_{\rm D} r_{\rm P}\phi(r_{\rm D},r_{\rm P})\Big]\frac{dV_{\rm P}}{dt} \\ &\qquad + 2\pi h r_{\rm D}\Big[c_{\rm P}\phi(r_{\rm D},r_{\rm P}) + c_{\rm D}\psi(r_{\rm D},r_{\rm P})\Big]\frac{dV_{\rm D}}{dt} \end{aligned} \tag{42}$$

where $c_{\rm M}(\lambda) = (1-\lambda)c_{\rm P} + \lambda\, c_{\rm D}$ and the auxiliary functions $\phi(x,y)$ and $\psi(x,y)$ are defined by

$$\begin{aligned} \phi(x,y) &= \frac{x}{6(x-y)^3}\left[x^2 - 5xy - 2y^2 + \frac{6xy^2}{x-y}\,\log\frac{x}{y}\,\right], \\ \psi(x,y) &= \frac{x}{6(x-y)^3}\left[2x^2 - 7xy + 11y^2 - \frac{6y^3}{x-y}\log\frac{x}{y}\,\right]. \end{aligned} \tag{43}$$

The evaluation of the integrals in expression (41) is facilitated by defining the auxiliary integrals

$$\mathcal{K}_1 = \int_0^1 \frac{(1-\lambda)^2\widehat{c}_{\rm M}(\lambda)\,d\lambda}{\widehat{r}(\lambda)}, \qquad \mathcal{K}_2 = \int_0^1 \frac{\lambda(1-\lambda)\widehat{c}_{\rm M}(\lambda)\,d\lambda}{\widehat{r}(\lambda)}, \qquad \mathcal{K}_3 = \int_0^1 \frac{\lambda^2\widehat{c}_{\rm M}(\lambda)\,d\lambda}{\widehat{r}(\lambda)}$$

and observing that $\mathcal{K}_1$, $\mathcal{K}_2$ and $\mathcal{K}_3$ can be determined easily from the identities

$$\begin{aligned} \mathcal{K}_1 + 2\mathcal{K}_2 + \mathcal{K}_3 &= \int_0^1 \frac{\widehat{c}_{\rm M}(\lambda)\,d\lambda}{\widehat{r}(\lambda)}, \\ r_{\rm P}\,\mathcal{K}_1 + r_{\rm D}\,\mathcal{K}_2 &= \int_0^1 (1-\lambda)\widehat{c}_{\rm M}(\lambda)\,d\lambda, \\ r_{\rm P}\,\mathcal{K}_2 + r_{\rm D}\,\mathcal{K}_3 &= \int_0^1 \lambda\,\widehat{c}_{\rm M}(\lambda)\,d\lambda. \end{aligned}$$

The results given in subsection 4.3.1 for a uniform segment ($r_{\rm P} = r_{\rm D}$) are obtained from formulae (42) by replacing $\phi(x,y)$ and $\psi(x,y)$ with their respective limiting values of 1/12 and 1/4 where each limit is taken as $x \to y$.

## Appendix 3 – Partitioning of voltage-dependent current on tapered cylinders

The construction of $I_{\rm P}^{\rm cap}$ and $I_{\rm D}^{\rm cap}$ for a membrane with non-constant specific capacitance provides the framework for treating intrinsic voltage-dependent transmembrane current. For tapered segments with non-constant membrane conductance, the contributions to the perturbations in the axial current at the proximal and distal boundaries of the segment are identical to expressions (42) with $c_{\rm P}$ replaced by $g_{\rm P}(V_{\rm P};\boldsymbol{\theta})$ and $c_{\rm D}$ replaced by $g_{\rm D}(V_{\rm D};\boldsymbol{\theta})$. These contributions are

$$\begin{aligned} I_{\rm P}^{\rm IVDC} &= 2\pi h\, r_{\rm P}\Big[g_{\rm P}(V_{\rm P};\boldsymbol{\theta})\,\psi(r_{\rm P},r_{\rm D}) + g_{\rm D}(V_{\rm D};\boldsymbol{\theta})\,\phi(r_{\rm P},r_{\rm D})\Big](V_{\rm P}-E) \\ &\quad + 2\pi h\Big[g_{\rm P}(V_{\rm P};\boldsymbol{\theta})\,r_{\rm D}\phi(r_{\rm P},r_{\rm D}) + g_{\rm D}(V_{\rm D};\boldsymbol{\theta})\,r_{\rm P}\phi(r_{\rm D},r_{\rm P})\Big](V_{\rm D}-E)\,, \\ -I_{\rm D}^{\rm IVDC} &= 2\pi h\Big[g_{\rm P}(V_{\rm P};\boldsymbol{\theta})\,r_{\rm D}\phi(r_{\rm P},r_{\rm D}) + g_{\rm D}(V_{\rm D};\boldsymbol{\theta})\,r_{\rm P}\phi(r_{\rm D},r_{\rm P})\Big](V_{\rm P}-E) \\ &\quad + 2\pi h\, r_{\rm D}\Big[g_{\rm P}(V_{\rm P};\boldsymbol{\theta})\,\phi(r_{\rm D},r_{\rm P}) + g_{\rm D}(V_{\rm D};\boldsymbol{\theta})\,\psi(r_{\rm D},r_{\rm P})\Big](V_{\rm D}-E) \end{aligned} \tag{44}$$

where the auxiliary functions $\phi(x,y)$ and $\psi(x,y)$ are defined in (43).

## Appendix 4 – Analytical solution for somal potential of test neuron

It may be shown that $V(t)$, the deviation of the somal transmembrane potential from its resting value as a result of a distribution $\mathcal{I}(x,t)$ of current on a uniform cylindrical dendrite of radius $a$ and length $l$ attached to a soma is

$$V(t) = e^{-t/\tau}\Big[\,\phi_0(t) + \sum_\beta\,\phi_\beta(t)e^{-\beta^2 t/L^2\tau}\,\cos\beta\,\Big]\,, \qquad L = l\sqrt{\frac{2g_{\rm M}}{ag_{\rm A}}} \tag{45}$$

where $\tau$ is the time constant of the somal and dendritic membranes and $g_{\rm M}$ and $g_{\rm A}$ have their usual meanings. The summation is taken over all the solutions $\beta$ of the transcendental equation $\tan\beta + \gamma\beta = 0$ where $\gamma$ (constant) is the ratio of the total membrane area of the soma to the total membrane area of the dendrite. The functions $\phi_0(t)$ and $\phi_\beta(t)$ are solutions of the differential equations

$$\begin{aligned} \frac{d\phi_0}{dt} &= -\frac{e^{t/\tau}}{C_{\rm D}+C_{\rm S}}\Big[\,\mathcal{I}_{\rm S}(t) + \int_0^l \mathcal{I}(x,t)\,dx\,\Big]\,, \\ \frac{d\phi_\beta}{dt} &= -\frac{2e^{(1+\beta^2/L^2)t/\tau}}{C_{\rm D}+C_{\rm S}\cos^2\beta}\Big[\int_0^1 \mathcal{I}(x,t)\cos\beta(1-x/l)\,dx + \cos\beta\,\mathcal{I}_{\rm S}(t)\,\Big] \end{aligned} \tag{46}$$

with initial conditions $\phi_0(0) = \phi_\beta(0) = 0$, that is, the neuron is initialised at its resting potential. The parameters $C_{\rm S}$ and $C_{\rm D}$ denote respectively the total membrane capacitances of the soma and dendrite, and $\mathcal{I}_{\rm S}(t)$ is the current supplied to the soma.

In the special case in which point currents $\mathcal{I}_1(t),\cdots,\mathcal{I}_n(t)$ act at distances $x_1,\cdots x_n$ from the soma of the uniform cylinder, the corresponding coefficient functions $\phi_0$ and $\phi_\beta$ satisfy

$$\begin{aligned} \frac{d\phi_0}{dt} &= -\frac{e^{t/\tau}}{C_{\rm D}+C_{\rm S}}\Big[\,\mathcal{I}_{\rm S}(t) + \sum_{k=1}^n \mathcal{I}_k(t)\,\Big]\,, \\ \frac{d\phi_\beta}{dt} &= -\frac{2e^{(1+\beta^2/L^2)t/\tau}}{C_{\rm D}+C_{\rm S}\cos^2\beta}\Big[\sum_{k=1}^n \mathcal{I}_k(t)\cos\beta(1-x_k/l) + \cos\beta\,\mathcal{I}_{\rm S}(t)\,\Big]\,. \end{aligned} \tag{47}$$